Wet Hydrogen Sulfide Cracking Monitoring by Acoustic Emission

Véronique Smanio[b], Marion Frégonèse [c], Jean Kittel [a],
Thierry Cassagne [b], François Ropital [a], Bernard Normand [c]

[a] *IFP, BP3 - 69360 Solaize – France*
[b] *TOTAL, CSTJF, Avenue Larribau – 64018 Pau cedex – France*
[c] *MATEIS, INSA-Lyon, CNRS UMR 5510, 69621 Villeurbanne cedex - France*
Email: veronique.smanio@ifp.fr

Abstract
Equipments which operate in wet hydrogen sulfide (H_2S) environment can be subjected to Hydrogen Embrittlement (HE) damages like Hydrogen Induced Cracking (HIC), Stress Oriented Hydrogen Induced Cracking (SOHIC), or Sulfide Stress Cracking (SSC). The resistance of steels to HIC and SSC is usually evaluated through standard tests (NACE TM0177 and NACE TM0284). These tests give operators and steel suppliers a pass/fail response for a given application.
However, the detailed mechanisms of wet H_2S cracking are not fully understood yet, although a lot of work has been carried out over the years on this subject. In particular it is of interest to better understand the initiation and propagation phases of HIC and SSC. For this purpose, some laboratory studies have used the acoustic emission (AE) technique to monitor the materials behaviour during HIC and/or SSC tests. Most of the results were promising, as some correlations were found between AE parameters and the cracking susceptibility of different materials. However, the most important gap stands in the analysis of AE data, which is always considered as a bulk, without any attempt to separate the contribution of other acoustic sources (such as general corrosion or hydrogen bubbling in the solution) from the cracking itself.
A methodology was developed in this work to discriminate HIC signals from other sources. The aim was to isolate the cracking contribution, and compare HIC propagation mode for different non sour service steels. In addition tensile tests monitored by AE on two sour service steels are also presented. Difference between SOHIC and SSC mechanisms could be evidenced by AE.

Introduction

Wet H_2S cracking of steels concerns a broad range of service applications in petroleum industry including oil and gas production, refining and gas processing.
Several kinds of damage may be caused by H_2S in contact with low alloyed steels [1].
In low strength plates and pipe steels, the main cracking process is Hydrogen Induced Cracking (HIC). HIC is caused by the accumulation of hydrogen at internal traps, such as non-metallic inclusions, regions of anomalous microstructures (e.g. pearlitic structure) produced by segregation of impurities and alloying elements, and other weak interfaces. When the concentration of hydrogen at the defects reaches a sufficient value, recombination to gaseous hydrogen occurs, with a build-up of high pressure leading to internal cracking. Under conditions of applied or residual tensile stresses, HIC cracks can become aligned in the through thickness direction resulting in 'ladder like' crack array referred as Stress Oriented Hydrogen Induced Cracking (SOHIC). This phenomenon is usually associated with low-strength ferritic pipe and pressure vessel steels.
The other kind of wet H_2S cracking mode studied in this work is Sulphide Stress Cracking (SSC). SSC leads to the early failure of the metal due to the combined effect of both hydrogen penetration and tensile stress (residual and/or applied). High strength metallic materials and

hard welded zones are prone to SSC. Crack initiation of SSC is always located at the surface of the metal.
The mechanisms of HIC and SOHIC are generally well accepted. On the other hand, the SSC mechanism is still controversial. Some authors [2,3] make the hypothesis that SSC is the result of hydrogen trapping, in a similar way to HIC. Traps would be located at high internal stress sites (i.e. grain boundaries, inclusions and regions of triaxial stress at notches). In the presence of tensile stress, these locations would become sites for embrittlement and could favour the initiation of brittle fracture. Other authors [4] suggest that SSC mechanism is caused by the powerful implantation of protons in the very first layers of metal which expands the crystal lattice. This expansion would generate a permanent surface tension. In addition to the working stress, this tension may then induce delayed cracking.

The main purpose of our study is to improve the understanding of cracking in wet H_2S media. In the past, several studies [5-10] have used Acoustic Emission (AE) technique to monitor Hydrogen Embrittlement (HE) in sour media. Weng et al. [5] found a correlation between HIC damage evaluated by Crack Length Ratio (CLR) [11] and the AE energy level. Most of the other studies were related to SSC and used AE monitoring during standard SSC tests described in NACE TM0177-96 [12]. Cayard et al. [6] and also Gingell et al. [7] showed that during SSC tests leading to the failure of the specimen, a higher AE energy build-up rate was recorded compared to no-failure tests. This critical energy build-up rate associated with SSC failure remained dependant on the tested steels and the applied stress level. Moreover, Gingell et al. [7] showed that AE could be used to discriminate initiation and propagation stages of SOHIC (Stress Oriented Hydrogen Induced Cracking) development.

From these studies, it appears that AE is a powerful tool for H_2S cracking evaluation. Some correlations can be found between the AE energy and the extent of cracking. However, for most of the past studies, the cracking mechanism was not always clearly established or documented, especially between SOHIC and SSC. Furthermore, AE data were treated in a global manner, i.e. considering simultaneously all the AE sources involved during the test. Considering this last point, a step forward was proposed recently by the authors [13-14]. A methodology was described, enabling to separate AE contributions from H_2 evolution due to acid corrosion, FeS layer build-up and evolution, and HIC. A correlation chart representing the absolute energy of the signals as a function of their duration was used for the discrimination (Figure 1).

Thus, it was possible to separate AE events related to HIC from the background noise, allowing a better analysis.

In the present work, this methodology was applied in order to compare HIC mechanisms of two different steels. It was also used for tests under tensile load allowing distinguishing SOHIC and SSC rupture modes.

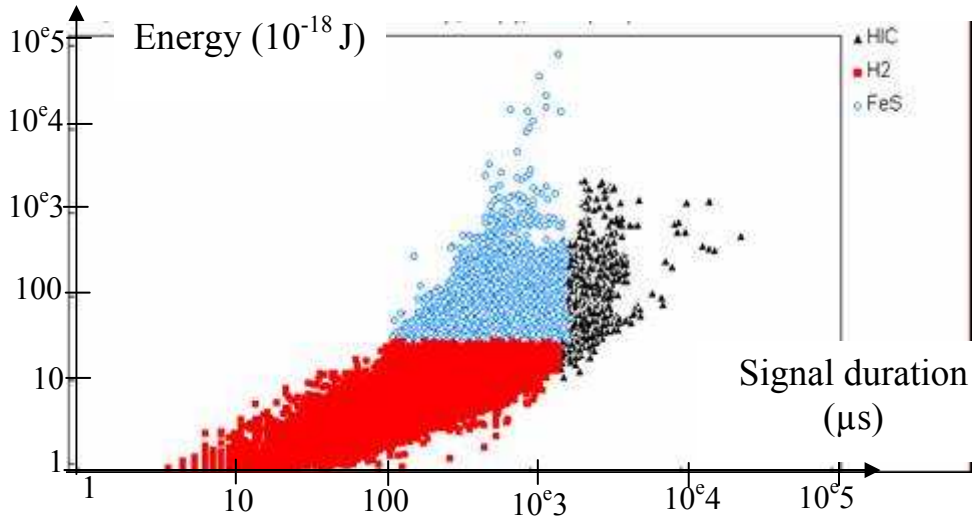

Figure 1: Correlation chart representing absolute energy as a function of signals duration for a test conducted in the EFC 16 solution at pH 4.5 under 1bar H_2S, on a X65 SwS specimen.

Experimental procedure

Experimental set up

The experimental set up (Figure 2) was based on the standard tensile test described in NACE TM0177-96 (method A) [12]. All tests were conducted with the same experimental set up. For HIC tests, no load was applied to the test specimens. For SSC or SOHIC tests, a constant strain was applied with the proof ring. Cylindrical tensile specimens were used for both study (HIC and SSC). Only the gauge section of the specimen was immersed in the corrosive solution. Tests were conducted in buffered solution prepared according to EFC 16 [15] (5 wt% NaCl and 0.4% CH_3COONa in distilled water) and under 1 bar H_2S. De-aeration of the solution was made by nitrogen bubbling ensuring less than 15 ppb dissolved oxygen before H_2S introduction.

A circulation of the corrosive fluid (sour media) was set-up between the test cell and a vessel, in which gas bubbling was maintained. This procedure allowed to avoid any interfering AE noise detection (e.g. gas bubbling in the test cell would result in AE) and to maintain constant the electrochemical conditions in the cell during the test (easier pH control). The pH was measured with a pH meter located in this second vessel and adjusted every day with HCl or NaOH additions.

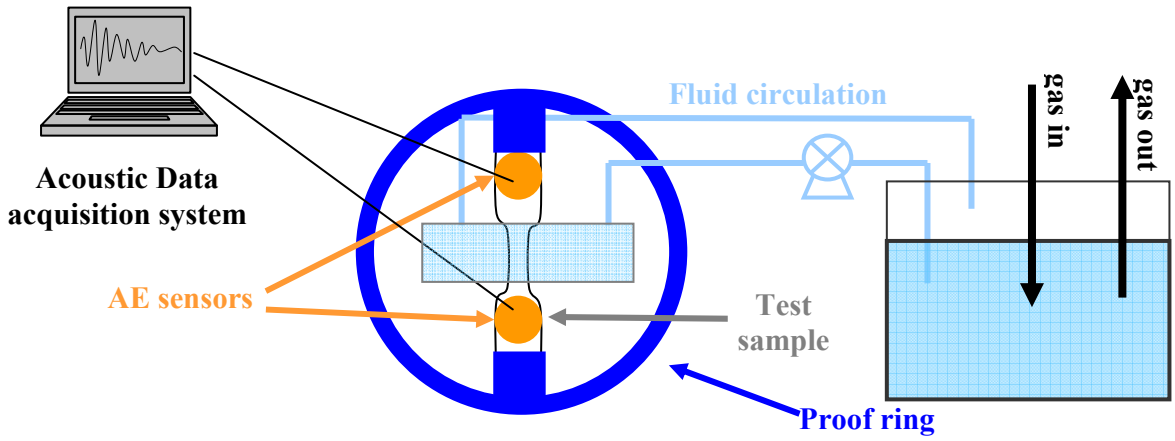

Figure 2: Experimental device.

AE monitoring was performed with two AE sensors placed at the top and bottom of the specimen (Figure 2). AE instrumentation consisted of a transducer, a preamplifier and a data acquisition system. The acquisition system was completely computer controlled. For each detected AE signal, online analysis was performed and several parameters were collected such as:

- Events number: number of AE signals detected (discontinuous emission),
- Amplitude: maximal amplitude of the considered AE event (peak),
- Rise time: time between the first overshoot of the defined threshold and the peak,
- Counts number: number of times that the threshold is overshot for a given AE event,
- Duration: time between the first and the last overshoot of the define threshold,
- Energy: envelop of the signal.

After HIC tests, damages in the specimen were evaluated by ultrasonic testing. From US scans, it is possible, with a software, to obtain an isosurface picture of the defects in the sample. In addition, metallographic examinations were made in three equidistant cuts along the length of the samples.
After SSC and SOHIC tests, fracture surfaces of SSC samples were examined by SEM (Scanning Electron Microscopy). A 3D reconstruction of the fracture surfaces was made using a Hirox 3D microscope. This microscope is motorized in z direction allowing taking several pictures of the fracture surface with different focus. Then, it is possible to reconstruct a full 3D picture of the fracture surface and to extract some profiles.

Materials

Four different steels were studied: three of them were low alloy steel plates for line pipe applications and the last one was a well tubing material. Two grades were Sweet Service (SwS) and two grades were Sour Service (SS).
The chemical compositions of all steels were analyzed by optical emission spectroscopy (OES), except for carbon and sulphur, analyzed by a chemical method (Table 1).

Table 1: Chemical composition (wt %) of steels.

Steel	C	Mn	Si	P	S	Cr	Ni	Mo	Cu	Nb
X65 (SwS)	0,09	1,56	0,28	0,014	0,001	0,05	0,03	0,01	0,02	0,040
X65 (SS)	0,046	1,36	0,322	0,008	0,001	0,041	0,036	0,008	0,047	0,045
X70 (SwS)	0,060	1,25	0,227	0,007	0,003	0,092	0,194	0,017	0,028	0,038
C110 (SS)	0,309	0,394	0,343	0,015	0,002	0,964	0,037	0,834	0,018	0,033

The line pipe steels X65 SwS, X70 SwS and X65 SS exhibit a low carbon content (<0,1%) compared to the C110 casing steel, which presents higher mechanical properties (Table 2). The C110 grade also contains alloying elements, such as chromium and molybdenum, providing a better resistance to hydrogen embrittlement.

The tensile properties of the steels in the longitudinal direction are given in Table 2.

Table 2: *Mechanical tensile properties of studied steels.*

Steel	YS(MPa)	UTS (MPa)	El%
X65 SwS	523	649	24
X65 SS	529	571	47
X70 SwS	548	615	28
C110 SS	798	887	20

(YS: Yield strength, UTS: Ultimate Tensile Strength, El: Elongation)

The microstructure of each steel was observed in the long transverse direction (LT) using an optical microscope, and after polishing down to 0.05µm diamond suspension and etching with a Nital solution (2%vol. nitric acid and ethanol). The different microstructures at the mid wall location are presented in Figure 3 to Figure 6.

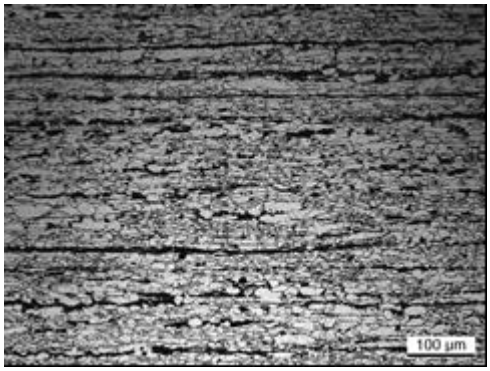

Figure 3: Microstructure of X65 SwS grade (LT plane).

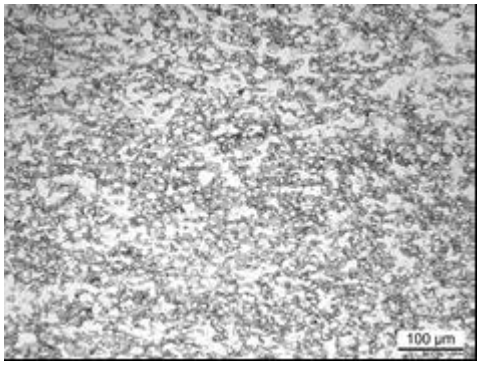

Figure 4: Microstructure of X65SS grade (LT plane).

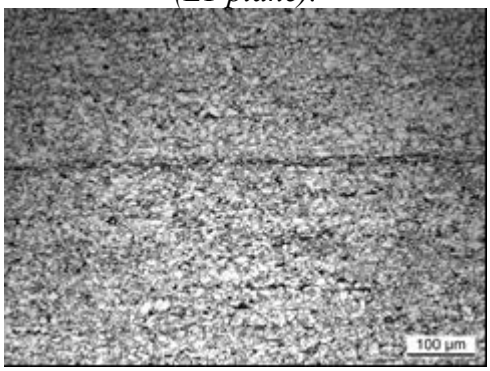

Figure 5: Microstructure of X70 SwS grade (LT plane).

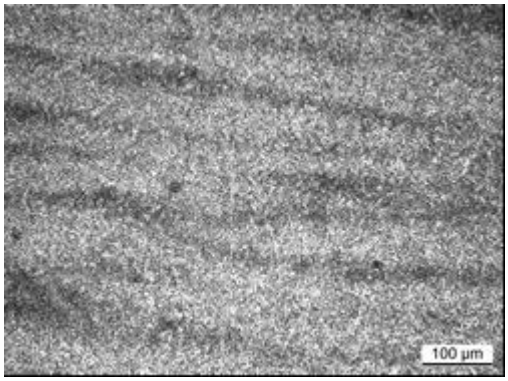

Figure 6: Microstructure of C110 SS grade (LT plane).

X65 SwS, X70 SwS and X65 SS has a ferrite pearlite microstructure. Microstructures of X65 SwS, X70 SwS are highly oriented in the rolling direction, which can affect their HIC resistance (Figures 3 and 5). Pearlite bands in X65 SwS are located on parallel planes at different width whereas X70 SwS steel exhibits only one pearlite band located in the middle plane of the sample.

For the X65 SS grade, the microstructure is equiaxed and homogenous, which explains its good HIC resistance (Figure 4).

The microstructure of C110 grade is a tempered martensite with macrosegregation (Figure 6). This microstructure is usually resistant to HIC [16].

Results and discussion

Acoustic emission was applied to compare HIC propagation in two sweet service steels (X65 SwS and X70 SwS grades) and then to identify the rupture mode under tensile stress, SSC or SOHIC, of both sour service steels (X65 SS and C110 SS grades).

HIC cracking behaviour of sweet service steels

HIC tests were performed on X70 SwS and X65 SwS at pH 4.5 under 1 bar H_2S and for 90 hours exposure.

All the AE data recorded during the tests were then filtered as described in [13,14], in order to keep only the events related to HIC. This procedure is illustrated in figure 7 for the experiment on the X70 SwS steel, and in figure 8 for the X65 SwS steel. Each point on these graphs represents an AE event. For this experimental configuration and AE equipment, the HIC events are characterized by durations above 1500 µs [13,14].

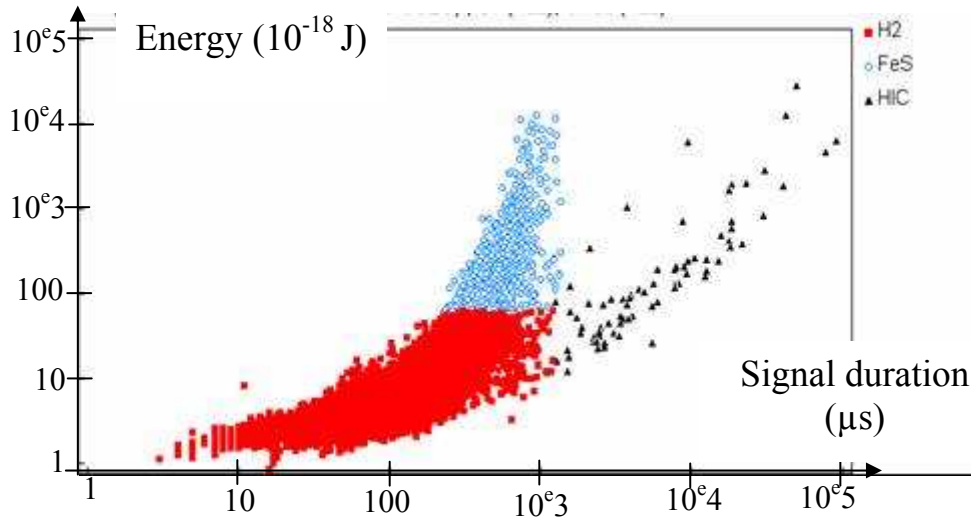

Figure 7: Correlation chart representing absolute energy as a function of signals duration for a test conducted in the EFC 16 solution at pH 4.5 under 1bar H_2S, on a X70 SwS specimen.

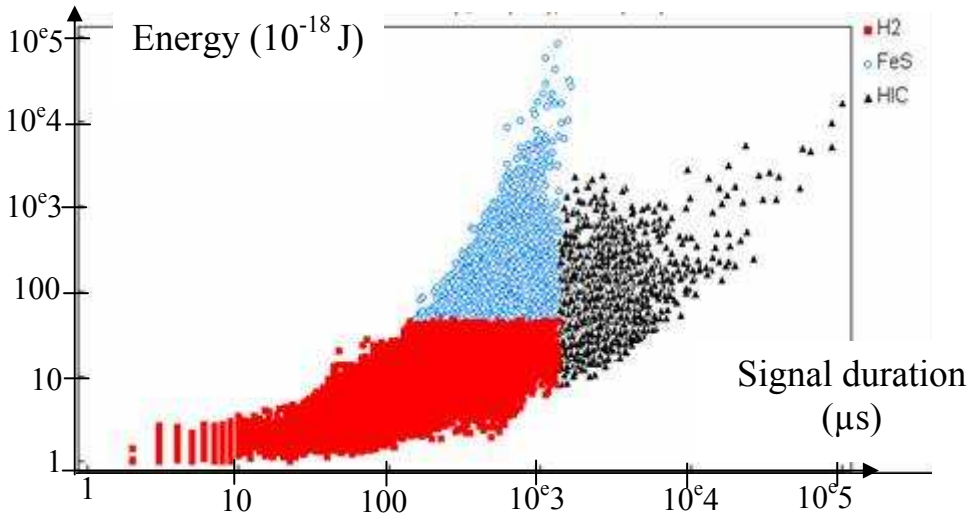

Figure 8: Correlation chart representing absolute energy as a function of signals duration for a test conducted in the EFC 16 solution at pH 4.5 under 1bar H_2S, on a X65 SwS specimen.

The comparison between Figure 7 and Figure 8 shows a difference in AE related to HIC for the two steels. More HIC signals were detected during the test performed on X65 SwS steel compared to the test done with the X70 SwS grade.

Once the filtering of AE data was performed, the evolution with time of HIC related signals was examined for X70 SwS steel (Figure 9) and for X65 SwS steel (Figure 10).

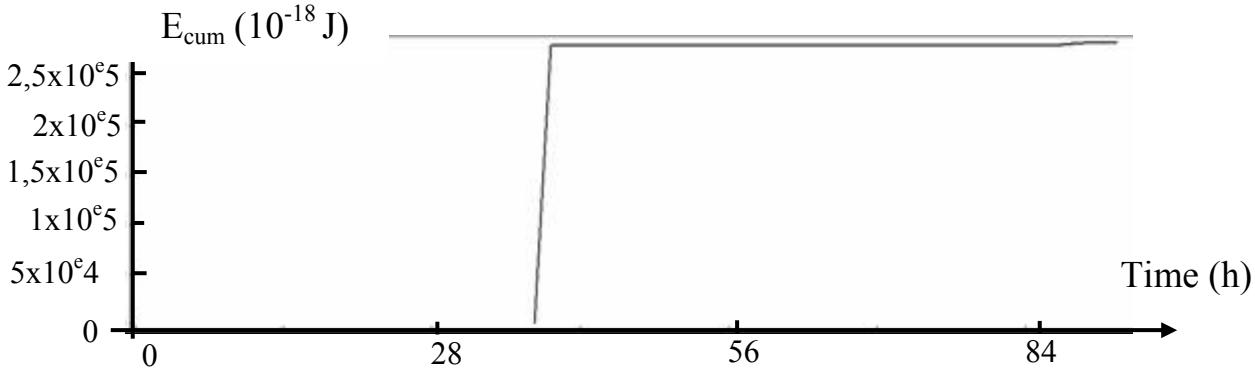

Figure 9: Evolution of cumulative energy of HIC class during a test performed on the X70 SwS steel grade at pH 4.5 under 1 bar H_2S.

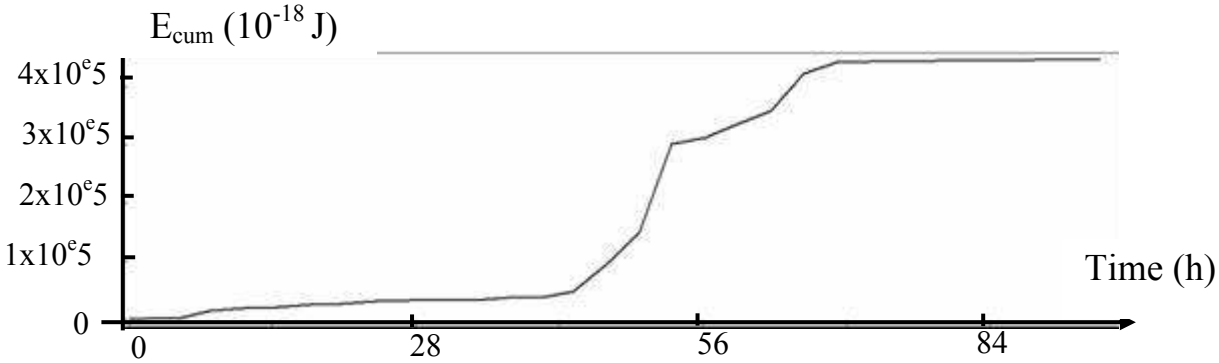

Figure 10: Evolution of cumulative energy of HIC class during a test performed on the X65 SwS steel grade at pH 4.5 under 1 bar H_2S.

The evolution of the AE energy related to HIC is clearly different for X70 SwS and X65 SwS. For the first steel, only one high energy jump is observed after 40 hours (Figure 9). On the other hand, AE signals related to HIC in X65 SwS proceed by successive steps between 43 hours and 68 hours. This difference may be explained by the number of cracks, by the difference in propagation path, or by different types of hydrogen traps in the steels.

After each test, ultrasonic testing was performed on the two samples. 3D reconstructions of the samples were made using US scans of X65 SwS (Figure 11) and of X70 SwS (Figure 12).

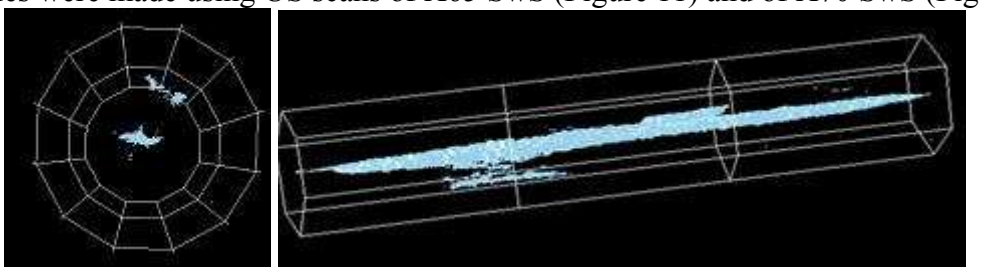

Figure 11: 3D picture of cracking in X70 SwS steel (reconstruction from US scan).

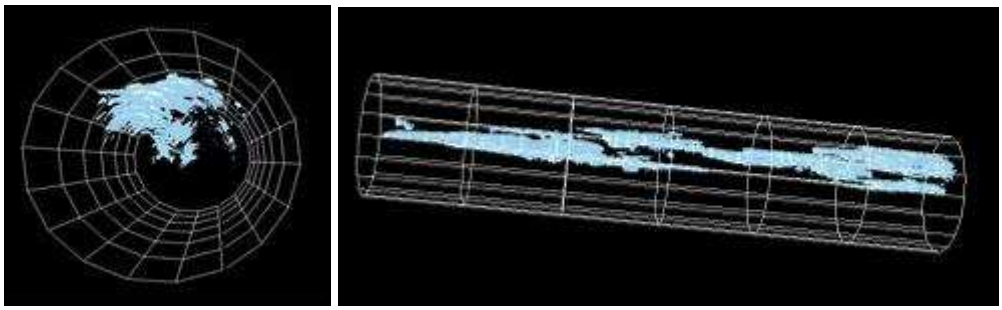

Figure 12: 3D picture of cracking in X65 SwS steel (reconstruction from US scan).

These representations give a global view of the damage state in the samples. For the X70 SwS, only one large crack is observed in the middle of the sample. On the other hand, 6 distinct cracks can be identified in the X65 SwS sample.

These results are confirmed by metallographic cross sectioning. Figure 13 shows the observation of cracks in L plan for X70 SwS and Figure 14 presents the longitudinal cross section for X65 SwS.

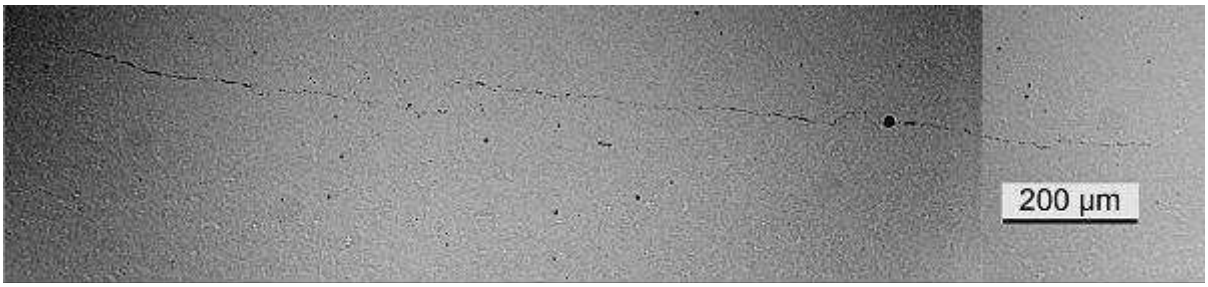

Figure 13: Metallographic observation of cracking in X70 SwS steel (L plan).

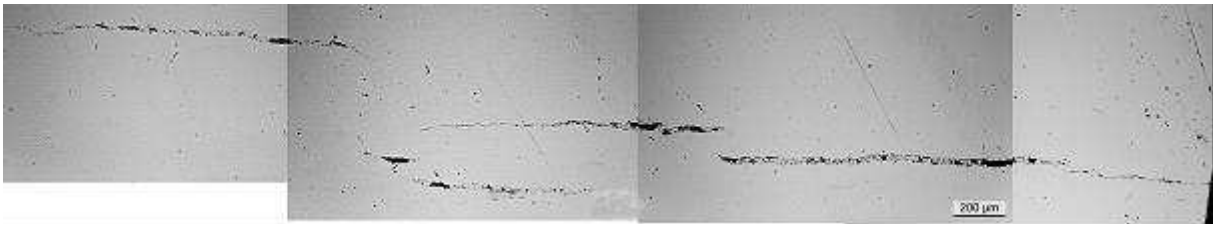

Figure 14: Metallographic observation of cracking in X65 SwS steel (L plan).

One main fine crack is identified in X70 SwS sample. Four large cracks can be observed by metallographic observations (Figure 14) inside the X65 SwS steel.

The difference in cracking damage in the two steels suggests that AE cumulative energy of HIC signals is correlated with HIC propagation. For the X70 SwS steel, one single crack propagates in the sample giving rise to one high AE energy jump. For the X65 SwS steel, several cracks propagate and result in several successive steps in cumulative energy evolution with time.

This comparison shows that AE provides real time information, not only on HIC kinetics but also on the details of the cracking. In this example, two types of cracking behaviours were identified. HIC in the X70 grade appears to be a single cracking event whereas X65 SwS seems to be multi-cracking. This difference in cracking might be explained by the difference in hydrogen trapping. The difference of cracking propagation seems to be related to the microstructure. X65 SwS steel presents multiple pearlite bands (Figure 3) whereas X70 SwS grade exhibits just one pearlite band in the middle of the sample (Figure5). In both steels, pearlite bands appear to be the main sites of hydrogen trapping leading to HIC.

In conclusion, AE seems to be a sensitive technique for the evaluation of HIC. The evolution of cumulative energy gives a foot print of the cracking process and information on HIC kinetics. Real-time information on the initiation, propagation and arrest of HIC can be obtained. In addition cracking modes (single or multiple cracking) can be identified.

Discrimination between SSC and SOHIC

Tests performed on X65 SS and C110 SS steels showed that these steels are not susceptible to HIC (no applied stress) at pH 3.5 under 1 bar H_2S. Then, tensile tests monitored by AE were made on these two sour service steels under the same conditions at 90% of actual YS.

AE results of the test conducted on X65 SS steel are represented in the correlation chart that was used for HIC discrimination, i.e. absolute energy versus duration of the signals (Figure 15).

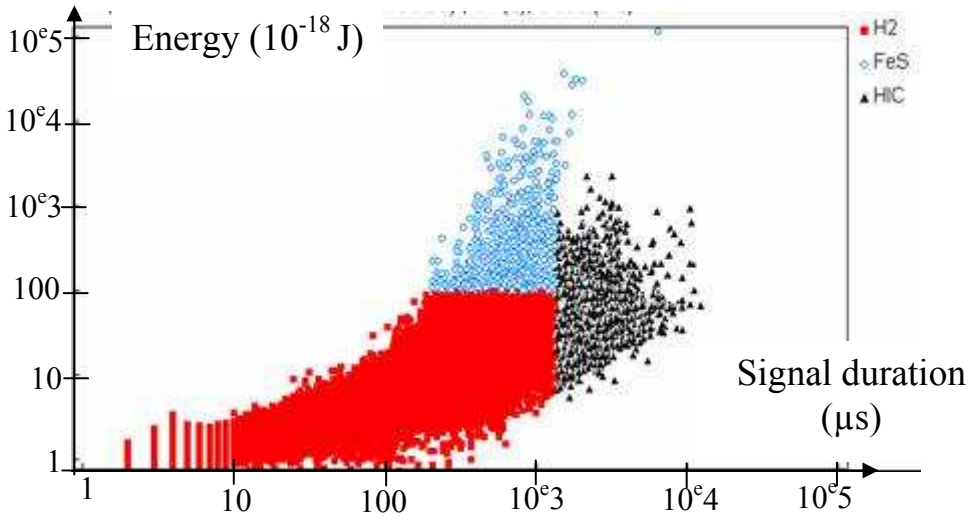

Figure 15: Correlation chart representing absolute energy as a function of signals duration for a test conducted in the EFC 16 solution at pH 3.5 under 1bar H_2S with an applied stress of 90% YS on a X65 SS specimen.

HIC signals were detected during the tensile test performed on the X65 SS steel. This was not the case during the test on C110 SS steel. Hence, from AE results, HIC cracks are expected in the X65 SS specimen.

SEM observation of the fracture surface of X65 SS is shown in Figure 16. Several internal cracks with a HIC appearance can be identified. Ductile microvoids can also be observed at higher magnification on the fracture surface (figure 20).

A profile of the fracture surface was extracted from a 3D reconstruction of the surface using a 3D microscope (Figure 17). The 45° rupture observed on this profile is typical of ductile fracture. Moreover, no perpendicular brittle flat fracture plane is observed.
From these observations, the fracture of X65 SS sample cannot be identified as SSC. The observed plastic deformation and the presence of internal cracks perpendicular to the fracture surface on one hand and the detection of HIC signals by AE on the other, strongly suggest a SOHIC mechanism in X65 SS under these test conditions.

Figure 18 shows the fracture surface of the C110 SS steel observed by SEM. Two areas can be identified. Fracture seems to initiate from the surface of the sample, and perpendicular to the loading direction (area 1). A trangranular fracture is observed in area 1 (figure 21) while microvoids are identified in area 2 (figure 22).
A profile of the fracture surface can be extracted from a 3D reconstruction of the surface using a 3D microscope (Figure 19). This profile is very different from the profile of the X65 SS sample. Area 1 which is brittle-like corresponds to a flat surface perpendicular to the direction of applied load. Area 2 identified as ductile corresponds to the 45° region.
This profile is typical of a SSC rupture. Sulfide stress cracking corresponds to the brittle area, then, as the section of the loaded part is reduced, the applied stress reaches the UTS and the sample fails by ductile fracture.

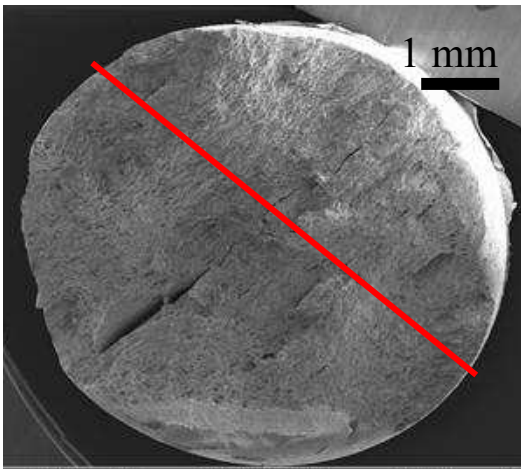

Figure 16: Fracture surface of X65 SS steel tested in the EFC 16 solution at pH 3.5 under 1bar H_2S with an applied stress of 90% YS.

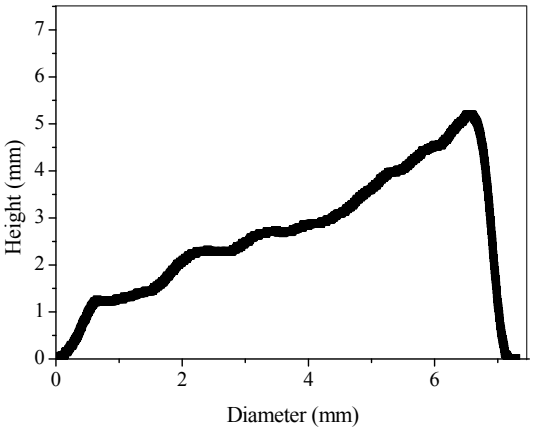

Figure 17: Profile of the fracture surface of X65 SS steel tested in the EFC 16 solution at pH 3.5 under 1bar H_2S with an applied stress of 90% YS. (red line on figure 16).

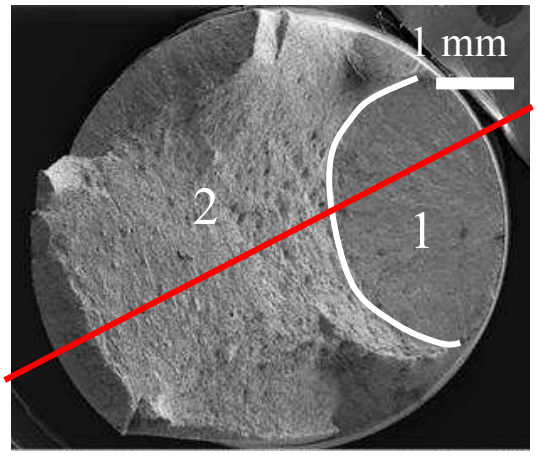

Figure 18: Fracture surface of C110 steel tested in the EFC 16 solution at pH 3.5 under 1bar H_2S with an applied stress of 90% YS.

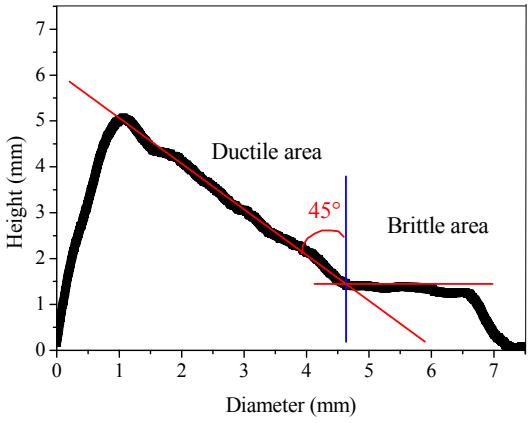

Figure 19: Profile of the fracture surface of C110 steel tested in the EFC 16 solution at pH 3.5 under 1bar H_2S with an applied stress of 90% YS. (red line on figure 17).

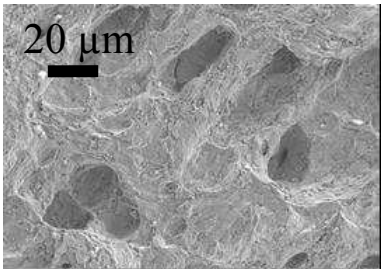

Figure 20: Detail of X65 SS fracture.

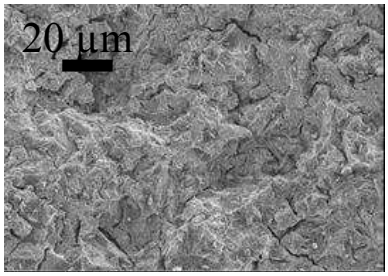

Figure 21: Detail of the brittle area of C110 fracture surface.

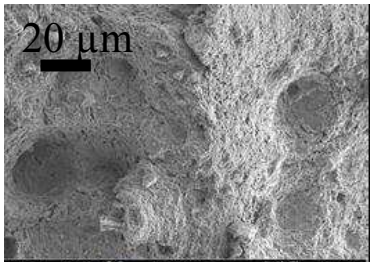

Figure 22: Detail of the ductile area of C110 fracture surface.

Two kinds of fracture have been presented. Fracture of X65 SS and C110 SS were identified as SOHIC and SSC, respectively. AE results of this two tests are different since in one case HIC signals were detected (X65 SS) and for the other one no HIC signals were detected (C110 SS). These results show that SSC and SOHIC fracture can be discriminated by AE. Moreover, SSC does not give rise to HIC signals and initiate on the specimen surface so it indicates that SSC is not related to subsurface trapping of hydrogen.

Sulfide stress cracking signals (not presented in this paper) exhibit a lower energy than HIC signals. Some indications to explain the difference observed between HIC and SSC signals can be inferred from the literature on stress corrosion cracking. Without forgetting that AE is dependent of each system it is possible to make a qualitative comparison of AE energy from different works.
Mc Intyre and Green [17] showed that intergranular fracture gives rise to higher energy AE events than transgranular fracture during stress corrosion cracking of steels. In the line pipe steel tested in this study, the HIC propagation mode at the ferrite/pearlite interface can be assimilated to an intergranular crack propagation, whereas for the C110 steel SSC leads to a transgranular fracture. This could explain the higher AE energy of HIC/SOHIC compared to SSC.
In addition, it is usually considered that the ability of crack detection is a function of crack velocity [18]. Higher velocity cracking such as cleavage give rise to higher energy AE signals. Therefore, a difference in crack velocity could also explain the difference in AE cracking detection between SSC and HIC/SOHIC.
In summary, the AE analysis confirms that different mechanisms of crack propagation are involved for HIC/SOHIC and SSC.

Conclusions

AE monitoring was applied to detect and analyse wet H_2S induced cracking modes in different steels in sour media, i.e. HIC, SSC and SOHIC. First, the discrimination of the different active AE sources during an HIC test such as H_2 evolution, FeS layer, and cracking was made. Then, this method was applied to study the HIC susceptibility of different steels. This method provides new information on the cracking kinetics but also helps to distinguish HIC cracking mode (single or multiple cracking).

Tests conducted under tensile stress monitored by AE technique were carried out in order to study SSC. It was found that SSC and SOHIC can be differentiated by AE analysis. SSC signals cannot be discriminated easily since they are less energetic than those associated with HIC. The AE analysis confirms that the SSC and HIC/SOHIC mechanisms are different.

In the future, HIC tests under mildly sour conditions will be conducted in order to better understand the influence of environmental parameters on the kinetics and extent of HIC. SSC initiation and propagation will also be investigated using AE.

Acknowledgement

Financial support from Total and IFP is gratefully acknowledged. The authors express their appreciation for assistance with the 3D observations of fracture surfaces to N. Mary from INSA-Lyon.

References

1. NACE MR0175/ISO 15156-2, **2003**.
2. G.M Pressouyre, J. Dollet, B. Vieillard-baron, *Mémoires et Etudes scientifiques Revue de métallurgie,* **1982,** *79*, 4.
3. R.D. Kane, M.S. Cayard, *NACE International Conference*, Houston, **1998,** paper n°274.
4. J-L. Crolet, *La Revue de Métallurgie*, **2004,** *101*, 12, 1053.
5. C-C. Weng, R-T. Chen, *Journal of the Chinese Institute of Engineers*, **1993,** *16*, 2, 195.
6. M.S. Cayard, R.D. Kane, *NACE International Conference*, Houston, **1997,** paper n°57.
7. A.D.B. Gingell, X.Garat, *NACE International Conference*, Houston, **1999**, paper n°600.
8. C-C. Weng, R-T. Chen, *Journal of Chinese Institute of Engineers*, **1993**, *16*, 4, 489.
9. S.Y. Tsai et H.C. Shih, *Journal of the Electrochemical Society,* **1998,** *145*, 6, 1968.
10. S. Amami, P. Marchand, S. Duval, X. Longaygue, M. Fregonese, H. Mazille, J.P. Millet, *Environmental Degradation of Engineering Materials*, Bordeaux, France, **2003.**
11. NACE International Standard Test Method NACE TM0284-96, *NACE*, **1996**
12. NACE International Standard Test Method NACE TM0177-96, *NACE*, **1996.**
13 V. Smanio-Renaud, M. Frégonèse, J. Kittel, T. Cassagne, F. Ropital, B. Normand, *Proceedings Eurocorr 2007*, Freiburg, Germany, **2007**.
14 V. Smanio, T. Cassagne, F. Ropital, J. Kittel, M. Frégonèse, B. Normand, *NACE International Conference*, Houston, **2008**, paper n°111.
15. S. Eliassen, L. Smith, P. Jackman, *Oil and gas production 2nd Edition European Federation of Corrosion (EFC number16),* **2002**.
16. J. Galland, J. Sojka, M. Jérome. *Prévention et lutte contre la corrosion* B. Normand, N. Pébère, C. Richard et M. Wery, Eds, Presses polytechniques et Universitaires Romandes, Lausanne, **2004**, 273.
17 P. McIntyre, G. Green, *British Journal of NDT*, **1978**, *20*, 135.
18 R. Rothéa, H. Mazille, *Corrosion sous contraintes : phénoménologie et mécanismes* D. Desjardins et R. Oltra, Eds, les éditions de la physique, **1990,** 515.